



ELSEVIER

Surface Science 313 (1994) 266–274

surface science

## Link between superstructures and kinetics in the Cu–Sb(100) system

H. Giordano <sup>a</sup>, J.P. Bibérian <sup>b</sup>, B. Aufray <sup>\*,a,b</sup>

<sup>a</sup> *Laboratoire de Métallurgie - CNRS, Université de Saint Jérôme, Case 511, Avenue Escadrille Normandie Niemen, 13397 Marseille Cedex 20, France*

<sup>b</sup> *CRMC2 - CNRS, Campus de Luminy, Case 913, 13288 Marseille Cedex 9, France*

(Received 17 December 1993; accepted for publication 14 March 1994)

### Abstract

We used dissolution and segregation kinetics to investigate the equilibrium superficial segregation of Sb on Cu(100). The kinetics are recorded by AES and the superficial superstructures determined from LEED patterns. Dissolution kinetics of one monolayer of Sb/Cu(100) stop for different superficial concentrations depending on the annealing temperature. Each superficial concentration corresponds to a particular superstructure which is indexed. A quasi-complete dissolution is obtained only for  $T = 770^\circ\text{C}$ . The segregation kinetics of Sb recorded at different temperatures on the surface of a Cu(Sb)(100) solid solution (0.2 at%) reveal different slow downs which are related to the different superstructures. The set of results is interpreted in terms of local equilibrium between the surface and the selvedge. A schematic “2D” phase diagram is proposed. The isotherm obtained at  $770^\circ\text{C}$  is compared to those obtained for S/Cu(100) at the same temperature. The results are discussed in the frame of the classical segregation theory.

### 1. Introduction

At a given temperature in a dilute alloy the surface segregation is the difference between bulk ( $C_b$ ; atoms/cm<sup>3</sup>) and surface solute concentrations ( $C_s$ ; atoms/cm<sup>2</sup>). This phenomenon is characterised by the segregation isotherm  $C_s = f(C_b)$  which describes all the equilibrium states. As shown by Laguës [1], and confirmed by recent

calculations in the framework of the kinetic tight-binding Ising model [2], the segregation isotherm can be inferred from the time dependence of the surface concentration of the segregating element. At a given temperature two kinds of kinetics  $C_s = f(t)$  can be studied:

- the segregation kinetics which corresponds to the solute out-diffusion towards the surface of an alloy.
- the dissolution kinetics which corresponds to the dissolution in the bulk of a thin film of solute deposited at room temperature on the pure metal.

A first study in a system presenting a tendency to phase separation (Ag/Cu) has demonstrated

\* Corresponding author. Present address: CRMC2 - CNRS, Campus de Luminy, Case 913, 13288 Marseille Cedex 9, France.

the unique ability of this kinetic approach to obtain an accurately superficial equilibrium segregation isotherm [3]. A recent study in the Sb/Cu(111) system has shown the limits of this kinetic approach for a system presenting a tendency to bulk ordering [4]. In this system the strong segregation of Sb leads to one stable superstructure which blocks the dissolution kinetics of Sb at 400°C so that only a part of the isotherm can be described by this kinetic procedure. It was then tempting, on one hand, to increase the temperature of the experiment in order to characterise the more complete as possible dissolution of Sb in the bulk and, on the other hand, to use a more open (100) crystallographic orientation for which a larger number of different superstructures is expected in order to characterise their influence on both dissolution and segregation kinetics.

In this paper we present new experimental data, obtained at different temperatures, concerning dissolution kinetics of an Sb submonolayer deposited on the Cu(100) face and segregation kinetics from a solid solution Cu(Sb)(100). The results are interpreted in terms of local equilibrium between the surface and the selvage. A schematic “2D” phase diagram is proposed. The isotherm obtained at 770°C is compared to those obtained for S/Cu(100) at the same temperature. The results are discussed in the frame of the classical segregation theory.

## 2. Experimental apparatus

The methodology used for the sample preparation is the same as previously described [3,5]. Let us recall some special points. The solid solution Cu(Sb)(100) with 0.20 at% of Sb is obtained by annealing a Cu single crystal at 900°C for one month in the presence of low-pressure Sb vapour. The experiments were performed in a standard AES-LEED system and the Auger spectra were acquired in the derivative mode. During the kinetics we systematically followed the Auger transition intensities for copper (60 eV and 920 eV), antimony (462 eV), oxygen (515 eV) and carbon (272 eV). Before annealing, the samples were

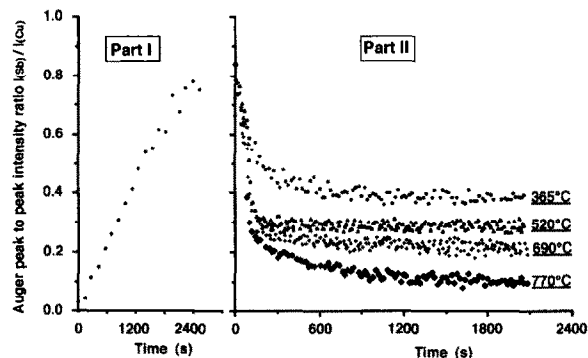


Fig. 1. Time dependence of the Auger peak-to-peak intensity ratio ( $I_{\text{Sb}}/I_{\text{Cu}}$ ). Part I: deposition at room temperature of 1 ML of Sb on Cu(100). Part II: dissolution kinetics of this deposit recorded at 365°C, 520°C, 690°C and 770°C.

cleaned by argon-ion sputtering at room temperature and then annealed a few minutes at 200°C in order to restore the surface. LEED observations and a complete spectrum (0 to 1000 eV) were always performed at room temperature at the beginning and at the end of each kinetics. The Sb was deposited in situ at room temperature by Joule heating of a crucible.

## 3. Results

The variations of Sb (462 eV) and Cu (60 eV) Auger peak-to-peak intensity ratios ( $I_{\text{Sb}}/I_{\text{Cu}}$ ) are displayed in Fig. 1. Part I illustrates an example of the deposition of about one monolayer (ML) of Sb at room temperature and Part II the dissolution kinetics in the bulk recorded just after this deposit for different temperatures. The deposition curves are classical but the shapes of the dissolution kinetics are surprising since in all cases the dissolution of Sb in the bulk is very fast at the beginning of the annealing and then stops for a given superficial concentration which depends on the annealing temperature. A quasi-complete dissolution of Sb is only observed for 770°C. Let us note that a complete Sb dissolution, which is the theoretical equilibrium state at the end of the kinetics, could only be observed after an infinite time of annealing since the lower the concentration gradient, the longer the dissolution

time. The LEED patterns observed at the end of each dissolution kinetics are shown in Fig. 2. The LEED pattern shown in Fig. 2d corresponds to a weak segregation of Sb observed during the cooling of the sample at the end of the quasi-complete dissolution recorded at 770°C.

In Fig. 3 the variations in the  $I_{\text{Sb}}/I_{\text{Cu}}$  ratio during the Sb segregation kinetics from a Cu(Sb) (100)-0.20at% alloy are plotted for almost the

same annealing temperatures. These kinetics present an increase of the Sb superficial concentration up to an asymptotic value which here also depends on the temperature. It is then interesting to remark that:

– The same value is reached for the ratio  $I_{\text{Sb}}/I_{\text{Cu}}$  (0.3, 0.4) for both segregation and dissolution kinetics. The ratio  $I_{\text{Sb}}/I_{\text{Cu}} = 0.2$  is never observed at the end of segregation kinetics.

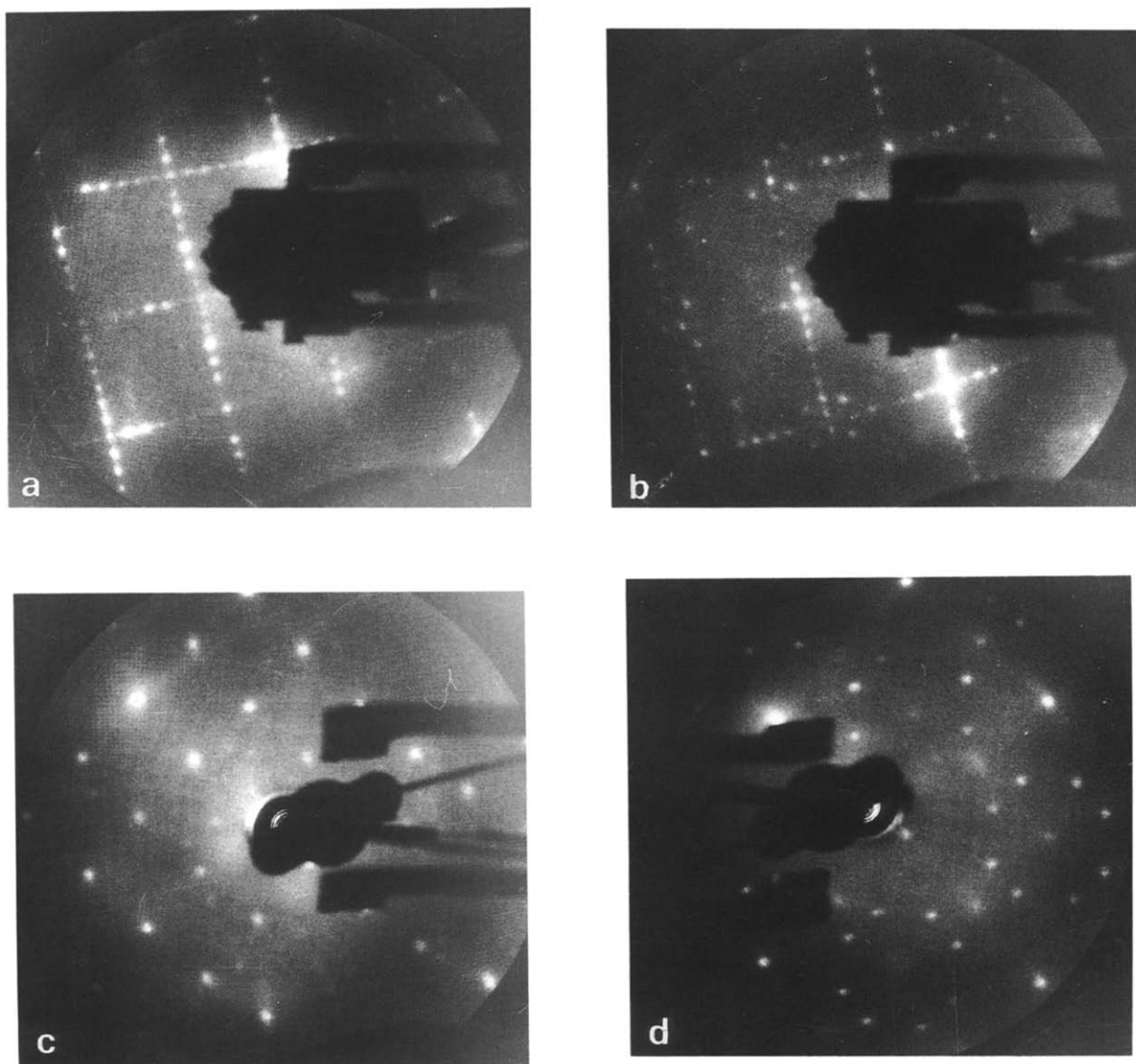


Fig. 2. LEED patterns observed at the end of the dissolution kinetics of 1 ML of Sb on Cu(100): (a) 365°C,  $E_p = 90$  eV; (b) 520°C,  $E_p = 70$  eV; (c) 690°C,  $E_p = 125$  eV; (d) 770°C,  $E_p = 90$  eV.

- On segregation kinetics different breaks can be observed before asymptotic values which are pointed on Fig. 3 by different arrows.
- The same LEED pattern as in Fig. 2a is observed at the end of all segregation kinetics recorded between 450°C and 375°C. At the end of the kinetics recorded at 355°C the observed LEED pattern corresponds to the one in Fig. 2b.

### 4. Discussion

#### 4.1. Superstructures

The growth mode of Sb on Cu(100) has been studied elsewhere by AES-LEED and RBS [6]

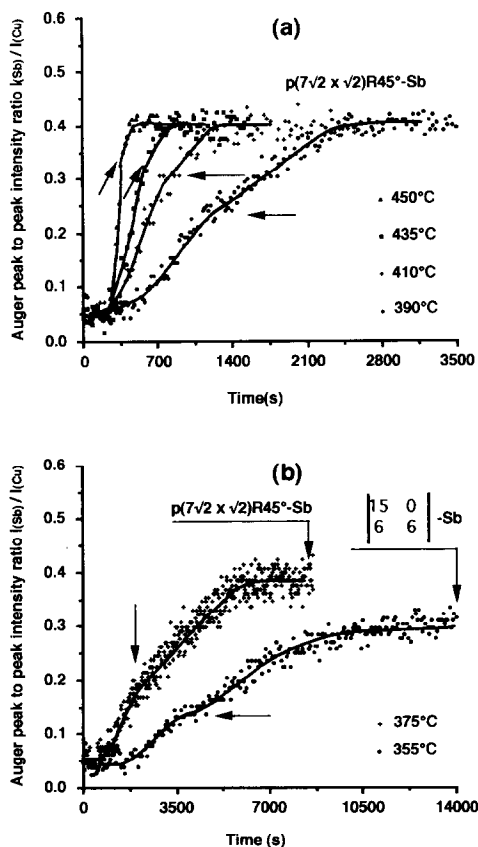


Fig. 3. Segregation kinetics from a 0.20 at% Cu(Sb)(100) solid solution: (a) 450°C, 435°C, 410°C and 390°C, (b) 375°C and 355°C.

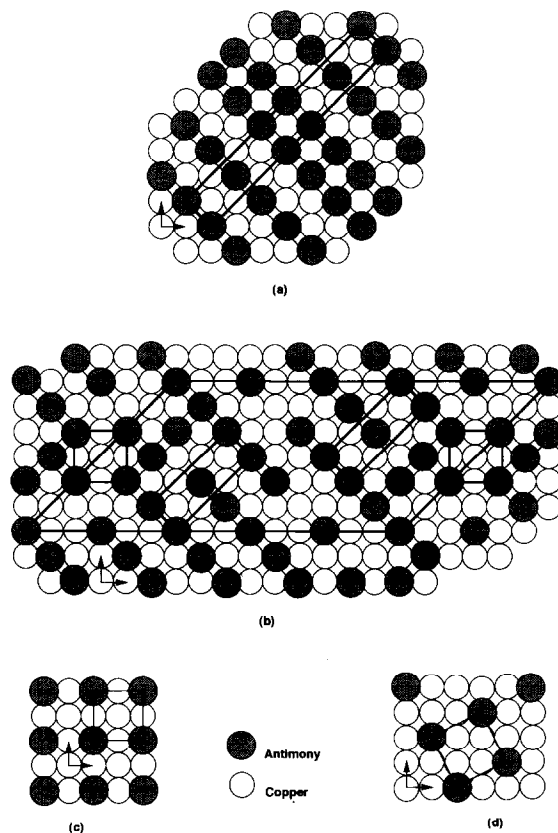


Fig. 4. Proposed surface structures deduced from the LEED patterns shown in Fig. 2: (a)  $p(7\sqrt{2} \times \sqrt{2})R45^\circ$ -Sb, (b)  $\begin{pmatrix} 15 & 0 \\ 6 & 6 \end{pmatrix}$ -Sb, (c)  $p(2 \times 2)$ -Sb, (d)  $p(\sqrt{5} \times \sqrt{5})R26^\circ$ -Sb.

and will not be discussed here. Let us just recall that the Sb monolayer is not ordered on the Cu surface and its density has been accurately evaluated to  $C_s = 1.0 \times 10^{15}$  atoms/cm<sup>2</sup> which corresponds to an attenuation of the Cu Auger (61 eV) signal intensity of 0.45 and an  $I_{Sb}/I_{Cu}$  ratio of 0.65. This calibration has been used to stop the deposit of Sb at about one monolayer (Fig. 1, Part I) and to evaluate the Sb superficial concentration corresponding to each superstructure.

The different superstructures shown in Fig. 4 are deduced from LEED patterns observed at the end of the dissolution kinetics. For each superstructure the number of Sb atoms per unit cell is derived from the results obtained by AES and then a possible arrangement of atoms in the unit cell is proposed. Note that the complex super-

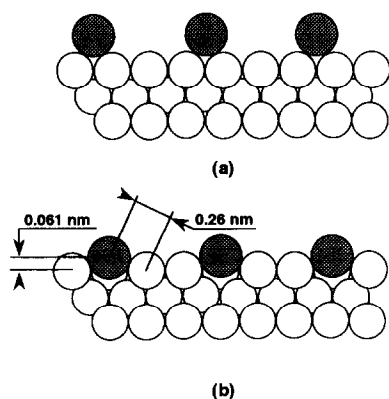


Fig. 5. Suggested structure for the  $p(7\sqrt{2} \times \sqrt{2})R45^\circ$ -Sb: (a) overlayer, (b) surface alloy.

structure deduced from the LEED pattern of Fig. 2b is ambiguous due to the absence of many spots. We have then used the main spots of the LEED diagram and propose an arrangement of Sb atoms in this superstructure which is a mixing of the two adjacent superstructures  $p(7\sqrt{2} \times \sqrt{2})R45^\circ$  and  $p(2 \times 2)$ . Table 1 recalls the superstructures obtained at the end of the dissolution kinetics and the corresponding Sb superficial concentration.

Due to the inaccuracy of AES measurements it is impossible from both deposition and dissolution curves to know if the surface layer is mixed Sb–Cu (Fig. 5b) or pure Sb (Fig. 5a). Nevertheless, the density of a pure Sb layer should be very weak ( $0.6 \times 10^{15}$ ) in comparison with a dense plane of Sb ( $1 \times 10^{15}$  atoms/cm<sup>2</sup>) [7] and should be energetically unfavourable in terms of surface tension. Furthermore, if one considers the relative interactions between nearest neighbours and

if we remember that Cu–Sb is a system presenting a tendency to bulk ordering, a mixed Sb–Cu layer is energetically more favourable (more neighbours and more Cu–Sb bounds) than a pure open Sb layer. With a classic model of hard spheres Fig. 5b shows the Sb atoms with a  $p(7\sqrt{2} \times \sqrt{2})R45^\circ$  superstructure forming schematically a “surface alloy”. It is interesting to see that this superficial structure can be regarded as a two-dimensional  $Cu_2Sb$  compound similar to the three-dimensional one which exists in the bulk phase diagram, however not with a fcc structure. In the bulk, the compression of Sb atoms can be relaxed by a structural modification (fcc  $\rightarrow$  A3) while the surface allows a relaxation of the simplest kind by an “up and down” (buckled) superficial reconstruction where Sb atoms are weakly higher in comparison to Cu atoms. This superficial structure has yet been proposed for adsorption of Sb on Ag(111) [8] and experimentally characterised by SEXAFS for Te deposited on Cu(111) at room temperature [9]. The Te atoms are found incorporated into the top Cu layer and situated at 0.081 nm above the ideal position. If one assumes a Cu–Sb bond length equal to that in  $Cu_2Sb$  compound, the Sb atoms should be 0.061 nm higher than for the ideal position.

#### 4.2. Dissolution kinetics

Let us now analyse the kinetic process of Sb dissolution and segregation in the frame of the usual Fick formalism that we will recall now.

If one assumes the existence of a local equilibrium [1,2] between the surface and the selvedge

Table 1  
Antimony superficial concentration corresponding to the observed superstructures

$I_{Sb}/I_{Cu}$	$C_s$ (atoms/cm <sup>2</sup> )	$T$ (°C)	Superstructure observed	Number of Sb atoms per unit cell
0.65	$1.0 \times 10^{15}$	Room temperature	Monolayer	
0.4	$0.6 \times 10^{15}$	365	$p(7\sqrt{2} \times \sqrt{2})R45^\circ$ -Sb	5
0.3	$0.45 \times 10^{15}$	520	$\begin{pmatrix} 15 & 0 \\ 6 & 6 \end{pmatrix}$ -Sb	27
0.2	$0.35 \times 10^{15}$	690	$p(2 \times 2)$ -Sb	1
	$0.30 \times 10^{15}$		$p(\sqrt{5} \times \sqrt{5})R26^\circ$ -Sb	1

( $x = 0$ ), it is possible to derive from the dissolution kinetics the concentration of dissolved atoms at time  $t$   $C_b(x = 0, t) = C_b(0, t)$  in equilibrium with the concentration of segregated atoms  $C_s(t)$ . For a dissolution process let us recall the general solution of the Fick diffusion equation for an “instantaneous” source at  $x = 0$ :

$$C_b(0, t) = \frac{M}{\sqrt{\pi D_b t}}, \quad (1)$$

where  $M$  is the quantity of atoms which penetrates in the bulk “instantaneously” and  $D_b$  the bulk diffusion coefficient of the solute.

If we consider (via local equilibrium hypothesis) that each elementary flux  $J_0(t)$  is equivalent to an “instantaneous source” through the surface then

$$C_b(0, t) = \frac{1}{\sqrt{\pi D_b}} \int_0^t J_0(t - \tau) \frac{d\tau}{\sqrt{\tau}}, \quad (2)$$

with  $J_0 = -dC_s(t)/dt$  which can be calculated from the experimental kinetics  $C_s(t) = f(t)$ . With formula (2) the dissolution kinetics allows us to compute the values of the Sb bulk concentration near the surface,  $C_b(0, t)$ , in equilibrium with the surface amount of Sb,  $C_s(t)$ . Let us recall that AES signal calibration of Sb is performed from a study of the growth mode [6] on Cu(100) and that we assume a linear variation of  $I_{Sb}/I_{Cu}$  with  $C_s(t)$  which is a good approximation due to the low Sb bulk solubility (3 at%). With  $D_b = 4 \times 10^{-14} \text{ m}^2 \text{ s}^{-1}$  (extrapolated from high-temperature measurements [10]) the “kinetic isotherm” derived from the dissolution kinetics recorded at 770°C is plotted in Fig. 6.

Let us first comment on the shape of this isotherm. As previously shown for the dissolution of Sb in Cu(111) [4] the “reentrant” shape is a consequence of the two different time regimes observed on the dissolution kinetics and, then, the first points of the “kinetic isotherm” are not characteristic of the equilibrium: they correspond to the path from the non-equilibrium initial condition towards local equilibrium. Because the dissolution is very fast at the beginning of the annealing, we cannot describe the concentration

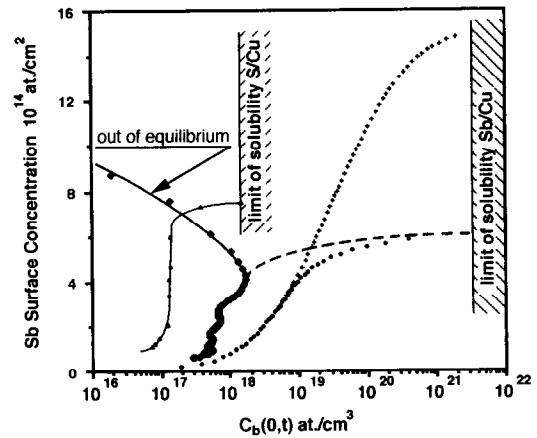


Fig. 6. Segregation isotherms  $C_s = f(C_b(0, t))$  of Sb/Cu(100) at 770°C: (◆ —◆): experimental (from dissolution kinetics); (— —): hypothetical range; (+): theoretical with a size effect independent of the surface concentration; (●): theoretical with a size effect dependent of the surface concentration; (▲ —▲) segregation isotherm of S/Cu(100) at 800°C (from Ref. [11]).

range from the solubility limit to the decreasing part of the isotherm (dashed line). On the bulk concentration scale the position of this isotherm ( $C_b(0, t) = 5 \times 10^{17} \text{ atoms/cm}^3$ ) is very low in comparison with the solubility limit at this temperature ( $3.5 \times 10^{21} \text{ atoms/cm}^3$ ). The oscillations observed on the isotherm are due to the polynomial fit used in order to calculate the integral of relation (2).

In Fig. 6 we also show the sulphur segregation isotherm on Cu(100) obtained at 800°C by radiochemical measurements by Petrino et al. [11]. One can see that the positions of both isotherms in the bulk concentration scale are close while the limits of the solubility are very different. This comparison clearly shows that the solubility limit is not always a reliable guide to predict accurately the segregation phenomenon [12]. In the case of systems with an ordering tendency (as Cu–S and Cu–Sb) the solubility limit is linked to the free enthalpy formation of the first compound from the solid solution one. Then, the “solubility limit” criterion can only be used for segregation prediction in systems presenting a tendency to phase separation. On the other hand, the vertical shape

of the S/Cu isotherm in comparison with the Sb/Cu one is probably linked to the difference in experimental techniques used. Indeed, as previously discussed by Lagües [1], the radiochemical technique used by Petrino et al. requires a cooling of the sample which necessarily increases the segregated quantities.

#### 4.3. Comparison with theoretical isotherms

Let us now compare this experimental isotherm Sb/Cu to the most common theoretical model [13] based on the assumption that segregation is limited to the first atom layer on which a simple regular solution approximation can be used:

$$\frac{X_s}{1 - X_s} = \frac{X_b}{1 - X_b} \exp \frac{-\Delta H}{RT}, \quad (3)$$

where  $X_{b(s)}$  is the bulk (surface) atomic fraction,  $T$  the temperature and  $\Delta H$  the segregation enthalpy which can be written as a sum of three terms:

– An interfacial energy term:

$$\Delta H_i = A(\Gamma_{Sb} - \Gamma_{Cu}). \quad (4)$$

– A chemical energy term calculated on the basis of a nearest neighbour bond model:

$$\Delta H_c = \frac{2\Delta H_m}{ZX_b(1 - X_b)} [Z_l(X_b - X_s) + Z_v(X_b - 0.5)]. \quad (5)$$

– A mechanical energy term  $\Delta H_w$  calculated from the atomic radii difference between atoms:

$$\Delta H_w = \frac{24\pi KGr_{Sb}r_{Cu}(r_{Sb} - r_{Cu})^2}{3Kr_{Cu} + 4Gr_{Sb}}. \quad (6)$$

In these relations  $A$  is the surface area per atom (of Cu),  $\Gamma_{Sb}$  and  $\Gamma_{Cu}$  are the surface energies of the pure components,  $\Delta H_m$  is the mixing enthalpy of the alloy,  $Z$  is the coordination number,  $Z_l$  is the number of lateral bonds in the surface plane,  $Z_v$  is the number of bonds with the first adjacent plane,  $K$  is the solute Young modulus,  $G$  the solvent shear modulus, and  $r_{Sb}$  and  $r_{Cu}$  are the atomic radii of the pure components.

In this description one postulates that the in-

Table 2

Parameters used for the calculation of the theoretical isotherm

	$G$ (J m <sup>-2</sup> )	$r$ (m)	$K$ (N m <sup>-2</sup> )	$G$ (N m <sup>-2</sup> )
Cu	1.825 [14]	$1.27 \times 10^{-10}$		$4.52 \times 10^{10}$ [15]
Sb	0.535 [14]	$1.45 \times 10^{-10}$	$5.49 \times 10^{11}$ [15]	

teractions between atoms are independent of the concentrations and that there is only one type of site. The segregation enthalpy  $\Delta H$  varies with  $X_s$ , but its variation only proceeds from the chemical term  $\Delta H_c$ . In this model the mechanical energy term  $\Delta H_w$  is assumed independent of the surface concentration.

Using the appropriate parameters for a dilute Cu(Sb) solid solution given in Table 2 and with  $2\Delta H_m/ZX_b(1 - X_b) = -16$  kJ/mol [16],  $Z_l = 4$  and  $Z_v = 4$  (for a (100) face), for (100) orientation we find the theoretical segregation isotherm at 770°C which is plotted in Fig. 6.

On the bulk concentration scale the position of this isotherm is in relative good agreement with the experimental one, but one can see a large discrepancy concerning the maximum of the superficial concentration. It can be attributed to the model which firstly assumes the same structure for the surface and the bulk and, secondly, a mechanical energy term independent of the surface concentration. This last assumption seems particularly crude when there is a large size difference between solute and solvent atoms. One can think that beyond a given surface concentration a total elastic energy relaxation (as assumed in relation (6)) is no longer possible. It is then more realistic to think that the elastic energy gain decreases with the surface concentration. This idea has yet been proposed for the interpretation of the shape of the Ag segregation isotherm on Cu [3,17]. In this system, which prevents a tendency to phase separation, the isotherm exhibits a vertical part interpreted as a “2D phase transition” until a superficial concentration of 0.5 ( $0.9 \times 10^{15}$  atoms/cm<sup>2</sup>). Above this concentration the isotherm exhibits a monotonous increase until the solubility limit. The calculation performed by

molecular dynamics in the tight-binding potential [17] shows a decrease of  $\Delta H_w$  as the square of the superficial concentration. Using a similar evolution for  $\Delta H_w$  with  $X_s$  in the case of Sb/Cu, the theoretical isotherm seems more realistic. From this point of view a comparison of the isotherm shapes for Sb/Cu and Ag/Cu in their upper parts is interesting and can be understood as follows. If we assume for both systems a gradual loss of the segregation driving force  $\Delta H_w$  with the solute surface concentration and if we remember the linear dependence of  $\Delta H_c$  with the superficial concentration then:

- For Ag/Cu,  $\Delta H_c$  is positive (favourable to the segregation of Ag atoms) and the upper part of the isotherm (for  $X_s > 0.5$ ) is the result of a competition between  $\Delta H_w$  and  $\Delta H_c$  when the superficial concentration increases.
- For Sb/Cu,  $\Delta H_c$  is negative (unfavourable to the segregation of Sb atoms) and the limit of the superficial concentration  $X_s = 0.34$  ( $0.6 \times 10^{15}$  atoms/cm<sup>2</sup>) is the result of a synergetic effect between  $\Delta H_w$  and  $\Delta H_c$ .

4.4. Segregation and dissolution kinetics

The dissolution kinetics recorded at 365°C, 520°C and 690°C can also be interpreted in the frame of the local equilibrium assumption. The shape of this kinetics, very fast bulk diffusion at the beginning of the annealing and then a blocking for a given superficial concentration, leads us to use Eq. (1) in order to calculate a part of the stability range corresponding to the different superstructures. We used the bulk diffusion coefficients measured at low temperature in the previous study [5]. The results of the stability range calculation are summarised in Table 3.

Table 3  
Stability range for the different observed superstructures

T (°C)	Superstructure observed	Stability range	
		$C_b$ (atoms/cm <sup>3</sup> )	$X_b$ (at%)
365	$p(7\sqrt{2} \times \sqrt{2})R45^\circ$ -Sb	$1 \times 10^{20} - 5 \times 10^{20}$	0.012–0.059
520	$(\begin{smallmatrix} 15 & 0 \\ 6 & 6 \end{smallmatrix})$ -Sb	$1 \times 10^{19} - 4 \times 10^{19}$	0.0012–0.047
690	$p(2 \times 2)$ -Sb	$1 \times 10^{18} - 4 \times 10^{18}$	0.00012–0.0047

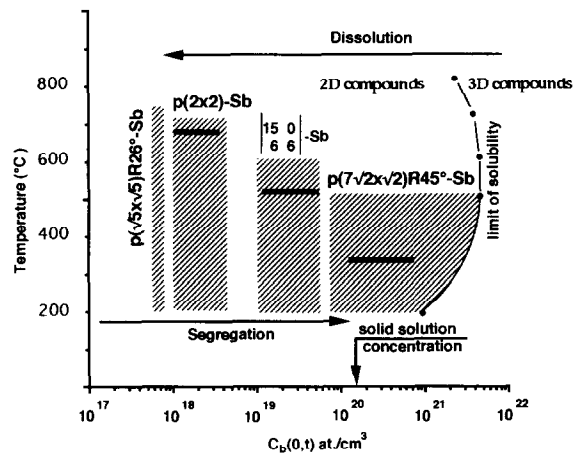


Fig. 7. Schematic “2D phase diagram”. The hatched areas show the stability range of the “2D compounds”. (—): Stability range determined from the dissolution kinetics.

It is very interesting to note that different superstructures can modify the segregation kinetics. More precisely, they lead to the slowing down of kinetics which are observed for superficial concentrations corresponding to the different superstructures. For a given temperature each superficial compound exists in a well defined bulk concentration range. With time there is a successive formation of the different compounds, but a superficial compound appears only when the concentration in the surface selvedge reaches the equilibrium value which characterises it. The observed slowing down is scarcely perceptible on the segregation kinetics. This is probably due to the small superficial concentration difference between successive superstructures. Furthermore, the concentration of the solid solution is always higher than the bulk concentration range in which this superstructure exists.

For the same reason this kinetics cannot be used to calculate a segregation isotherm: the concentration of the solid solution remains always higher than the concentration  $C_b(0, t)$  in the selvedge. Nevertheless, this segregation kinetics shows that the different superficial compounds which are characterised by dissolution exist also at low temperature where they lead to a different slowing down on the kinetics.

Therefore, from this set of results, it is possible to schematically draw a “2D phase diagram” of the Sb segregation on the (100) face of Cu. On this diagram (Fig. 7) we report the different concentration and temperature ranges on which the superficial compounds are in local equilibrium. We also plot the solubility limit of Sb in Cu which can be considered as the border between the “3D” and “2D” compounds. This diagram is obviously not very accurate since the borders between the different “2D” compounds are unknown. For the sake of clarity of this diagram, let us note that during a dissolution process one follows the phase diagram from the right to the left (from the solubility limit to low bulk concentrations) and during a segregation process from the left to the right (from low bulk concentrations to the solid solution concentration).

## 5. Conclusion

We have used dissolution and segregation kinetics to investigate the equilibrium superficial segregation of Sb on Cu(100). Dissolution kinetics of about one monolayer of Sb/Cu(100) stop for different superficial concentrations depending on the annealing temperature. Each superficial concentration corresponds to a particular superstructure on which a crystallographic arrangement of Sb atoms in the unit cell is proposed. An almost complete dissolution is obtained only for  $T = 770^\circ\text{C}$ . On the other hand, the segregation kinetics of Sb, recorded at different temperatures on the surface of a Cu(Sb)(100) solid solution (0.2 at%), reveals different slow downs which correspond to the formation of the different superstructures. Finally, the interpretation of the set of results in terms of local equilibrium between the surface and the selvedge leads us to propose a schematic “2D” phase diagram separating the existence ranges of these various superstructures.

## Acknowledgements

We would like to gratefully acknowledge G. Tréglia for critically reading this manuscript. We also thank B. Legrand, C. Mottet and A. Saul for many helpful discussions.

## References

- [1] M. Laguës and J.L. Domange, *Surf. Sci.* 47 (1975) 77; M. Laguës, *Philips Res. Rep.*, suppl. 5 (1976).
- [2] A. Senhaji, G. Tréglia, B. Legrand, N.T. Barrett, C. Guillot and B. Villette, *Surf. Sci.* 274 (1992) 297; A. Senhaji, G. Tréglia, J. Eugène, A. Khoutami and B. Legrand, *Surf. Sci.* 287/288 (1993) 371.
- [3] J. Eugène, B. Aufray and F. Cabane, *Surf. Sci.* 241 (1991) 1; 273 (1992) 372.
- [4] H. Giordano and B. Aufray, *Surf. Sci.* 307–309 (1994) 816.
- [5] H. Giordano, O. Alem and B. Aufray, *Scr. Met.* 28 (1993) 257.
- [6] H. Giordano, B. Aufray, C. Cohen, D. Schmaus, F. Abel, A. l’Hoir and Y. Girard, to be published.
- [7] F. Jona, *Surf. Sci.* 8 (1967) 57.
- [8] T.C.O. Noakes, D.A. Hutt and C.F. McConville, *Surf. Sci.* 307–309 (1994) 101.
- [9] F. Comin, P.H. Citrin, P. Eisenberger and J.E. Rowe, *Phys. Rev. B* 26 (1982) 7060.
- [10] V.A. Gorbachev, S.M. Klotsman, Y.A.A. Rabovskov, V.K. Talinskiy and A.N. Timofeyev, *Phys. Met. Metall.* 35 (1973) 4.
- [11] P. Petrino, F. Moya and F. Cabané, *J. Solid State Chem.* 2 (1970) 439.
- [12] E.D. Hondros, M.P. Seah, *Met. Trans. A* 8 (1977) 1363; F. Cabané and J. Cabané, *J. Phys. (Paris)* 49 C5 (1988) 423.
- [13] P. Wynblatt and R.C. Ku, *Surf. Sci.* 65 (1977) 511.
- [14] F.R. de Boer, R. Boom, W.C.M. Mattens, A.R. Miedema and A.K. Niessen, *Cohesion in Metals: Transition Metal Alloys*, Vol. 1 (North-Holland Amsterdam, 1988).
- [15] K.A. Gschneidner, *Solid State Phys.* 16 (1964) 275.
- [16] R. Hultgren, P.D. Dessai, D.T. Hawkins, M. Gleiser and K.F. Kelley, *Selected Values of the Thermodynamic Properties of the Elements* (American Society of Metals, Cleveland, OH, 1973).
- [17] G. Tréglia, B. Legrand, J. Eugène, B. Aufray and F. Cabané, *Phys. Rev. B* 44 (1991) 5842.